STRUCTURAL EFFECT OF UHPC DUCTILITY

Eugene Chuang, PhD, PE, Dept. of Civil Engineering, Massachusetts Institute of Technology, Cambridge, MA
Hesson Park, Dept. of Civil Engineering, Massachusetts Institute of Technology, Cambridge, MA
Franz-Josef Ulm, PhD, Dept. of Civil Engineering, Massachusetts Institute of Technology, Cambridge, MA

ABSTRACT

Previous research has proven the suitability of a UHPC model and corresponding finite element implementation for predicting the global and local behavior of UHPC structures. Using the finite element implementation of this UHPC model, the link between UHPC ductility and structural performance is elucidated with a sensitivity analysis of UHPC ductility parameters - invariants which quantify ductility at the UHPC material level. With this sensitivity analysis, one may compare the ductility offered by UHPC to that of other materials at a structural level. For instance, by reducing the ductility through material parameters, one may predict the structural behavior of a less ductile cementitious material. Conversely, by improving ductility, the possible structural gains through future material improvements can be envisioned.

Keywords: High Performance Concrete, Ductility, Material Modeling, Structural Modeling

INTRODUCTION

Ultra-high performance concrete (UHPC) is a fiber reinforced cementitious material which offers many advantages over normal concrete for prestressed concrete applications, such as high compressive strengths, low creep, and negligible autogeneous shrinkage[1,2]. The elasto-plastic tensile behavior of UHPC is particularly beneficial as it may allow for the elimination of shear reinforcement and passive reinforcement in many UHPC beam applications. However, the high cost of UHPC materials renders them economically inefficient for some prestressed concrete applications. Therefore, the structural effect of UHPC ductility should be evaluated before its employment.

A previously presented UHPC model and corresponding finite element implementation may be utilized for the structural evaluation of UHPC ductility. The UHPC model is a two-phase model, one phase representing the cementitious matrix and the other representing the reinforcing fibers, which is characterized by 10 material parameters of clear physical importance[3]. The finite element implementation of the model was shown to provide reliable and relevant predictions of load-deflection behavior, local strain behavior, and cracking behavior for two structural case studies: a flexural girder and a shear girder which have been recently tested by the FHWA[4].

Using finite element (FE) simulations, this paper elucidates the link between UHPC ductility and structural performance with a sensitivity analysis of UHPC ductility parameters - invariants which quantify ductility at the UHPC material level. With this sensitivity analysis, one may compare the ductility offered by UHPC to that of other materials at a structural level. For instance, by reducing the ductility through material parameters, one may predict the structural behavior of a less ductile cementitious material. Conversely, by improving ductility, the possible structural gains through (future) material improvements can be envisioned. This examination begins with a review of the UHPC model.

MATERIAL MODEL AND INPUT PARAMETERS

THE 1-D UHPC MODEL

Figure 1 displays the typical material response of UHPC materials obtained from a displacement driven notched tensile plate test. Following an initial elastic domain (A-B), the matrix cracks, which manifests itself as a macroscopic stress drop. However, this stress drop is mitigated by the redistribution of the stresses at the level of the composite materials, i.e. matrix and fibers. As a consequence, the overall composite material exhibits an apparent hardening behavior (B-C) until a macroscopic tensile yield strength is achieved. While the application of the tensile strength of cementitious materials is often restricted by the uncertainty regarding their tensile values, careful batching and mixing procedures for UHPC results in less dispersive tensile values, allowing safe exploitation of the tensile and shear capacity of UHPC in structural applications.

To capture this physically observed UHPC macroscopic behavior, a two-phase model, which is displayed in Figure 2, is employed. This model was formulated not only to capture physically observed macroscopic behavior, but also micromechanical processes (such as elasticity, cracking, and yielding) which occur at a level below. In this model, developed in

detail by Chuang and Ulm[3], a brittle-plastic composite matrix phase (stiffness C_M, brittle strength f_t, plastic strength k_y) is coupled to an elasto-plastic composite fiber phase (stiffness C_F, strength f_y) by means of a composite interface spring (stiffness M). This composite interface spring is not activated until cracking occurs in the composite matrix phase. Figure 1 compares the stress-strain response of the 1-D model with the experimentally determined UHPC stress-strain relation. Figure 3 shows the individual evolutions of the composite matrix stress σ_M and the composite fiber stress σ_F when an external tensile strain E is imposed.

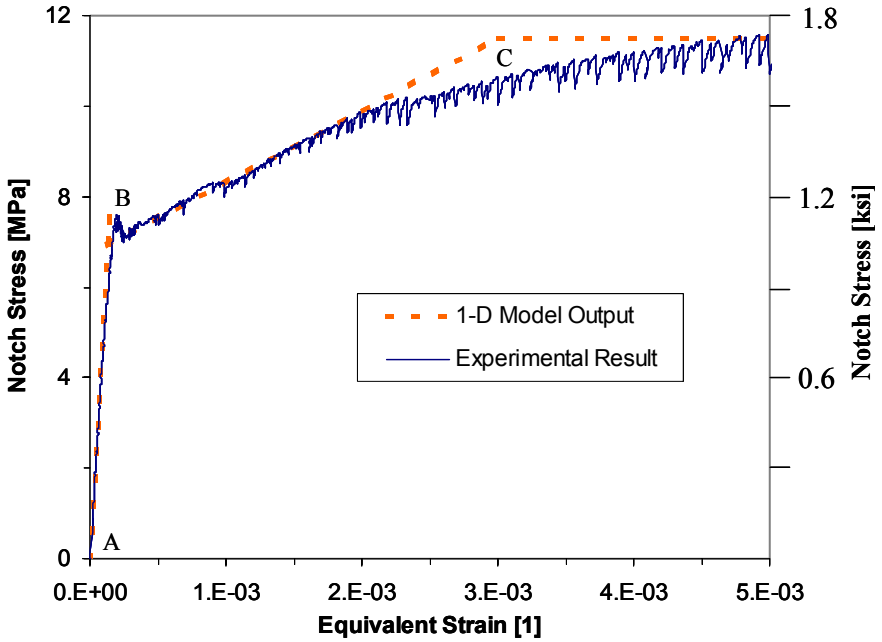

Fig. 1 Tensile Stress-Strain Curve for the UHPC Specimen (Experimental Data from Lafarge) and the Corresponding 1-D UHPC Model

It is important to note that the term 'phase' employed here does not necessarily refer to micromechanical phases in the material at smaller scales. Rather, one may consider the fiber phase as a macroscopic representation of the stiffness (stiffness C_F) and yield capacity (yield strength f_y) that are added to the overall UHPC composite stiffness and strength due to the addition of reinforcing fibers, which are activated (via the coupling spring M) upon matrix cracking. However, the composite matrix plastic strains ε_M^p which form during loading can be directly related to UHPC crack widths which are physically observed in loaded specimens, as shown in subsequent sections.

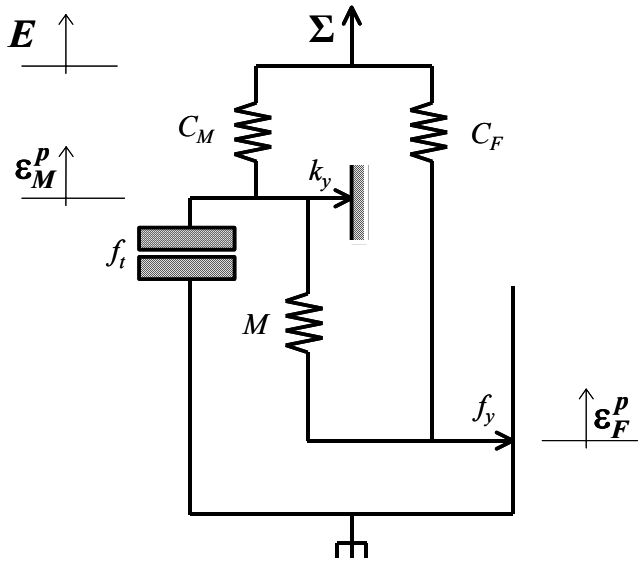

Fig. 2 The 1-D UHPC Model[3]

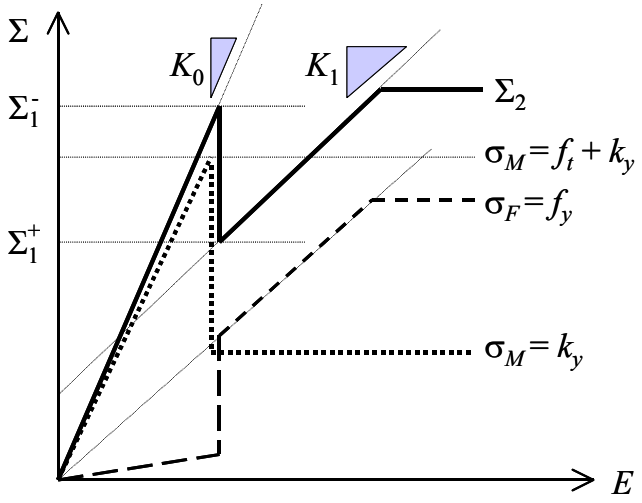

Fig. 3 Individual Responses of the Composite Matrix and Composite Fiber During Tensile Loading

EXTENSION OF THE 1-D MODEL TO 3-D

The extension of the 1-D model to 3-D requires three main components:

- A 3-D stress-strain relationship which is derived from energy considerations for a stress-strain expression which is thermodynamically consistent with the 1-D result.
- Strength domain: unlike the 1-D UHPC strength domain, which is only described by the tensile strength limits of the UHPC material, the 3-D strength domain requires 3-D strength limits, that is tension, compression, shear, etc.

- 1-D consistency condition: finally, for consistency with the 1-D UHPC model, the uniaxial behavior (stress loading in only one direction) of the 3-D model is calibrated with the 1-D UHPC model response (see Fig. 1). In this way, the 3-D model exhibits a tensile response which is thermodynamically consistent with that of the 1-D UHPC model.

Isotropic stress-strain relationships and strength domains are applied to the 3-D UHPC model. While isotropy is selected for the sake of simplicity, validation of the model shows this assumption to be quite adequate. The detailed development of the 3-D extension is given by Chuang and Ulm[4].

Model Parameter	Description	DUCTAL™ Value
C_M [ksi (GPa)]	Stiffness of the composite matrix	7820 (53.9)
C_F [ksi (GPa)]	Stiffness of the composite fiber	0 (0)
M [ksi (GPa)]	Stiffness of the composite interface	240 (1.65)
ν_M [1]	Poisson's ratio of the composite material	0.17
f_t [ksi (MPa)]	Brittle tensile strength of the composite matrix	0.1 (0.7)
k_y [ksi (MPa)]	Post-cracking tensile strength of the composite matrix	1 (6.9)
σ_{Mc} [ksi (MPa)]	Initial compressive strength of the composite matrix	28 (190)
σ_{Mb} [ksi (MPa)]	Initial biaxial compressive strength of the composite matrix	32 (220)
f_y [ksi (MPa)]	Tensile strength of the composite fiber	0.67 (4.6)
σ_{Fc} [ksi (MPa)]	Compressive strength of the composite fiber	1.5 (10)

Table 1 Parameters of the 3-D UHPC Model and Corresponding Values for DUCTAL™

SUMMARY OF MODEL PARMETERS

In addition to the 1-D model parameters (C_M, f_t, k_y, C_F, f_y, M), the 3-D UHPC model employs four parameters: Poisson's ratio ν_M, composite matrix compressive strength σ_{Mc}, composite matrix biaxial compressive strength σ_{Mb}, and composite fiber compressive strength σ_{Fc}. This yields a total of 6 + 4 = 10 model parameters summarized in Table 1 which can be determined through a single tensile test, a single compression test, and commonly accepted cementitious data[4]. Also listed in the table are parameter values determined for DUCTAL™, a UHPC material produced by Lafarge which is used in the FHWA girders and whose ductility parameters are used for the "Base Case" for the sensitivity analysis.

VALIDATION OF THE 3-D MODEL: A REVIEW

To validate the UHPC model and its finite element implementation, two tests performed by the FHWA were investigated (FHWA, 2002). Both tests involved AASHTO Type II girders (see Fig. 4(a)) comprised of DUCTAL™ without shear reinforcement:

- FHWA flexure test. A prestressed girder with a 78.5 ft (23.9 m) long test span was loaded in four point bending with two equal load points (total load P) located 3 ft (0.9 m) from the midspan (see Fig. 5(Top)).
- FHWA shear test. A 14 ft (4.3 m) girder was tested in three point bending, as illustrated in Fig. 5(Bottom). The load P was applied off-center, 6 ft (1.8 m) from one of the supports, in order to induce high shear stresses in the short load span.

For the complete validation of the UHPC model, refer to Chuang and Ulm[4].

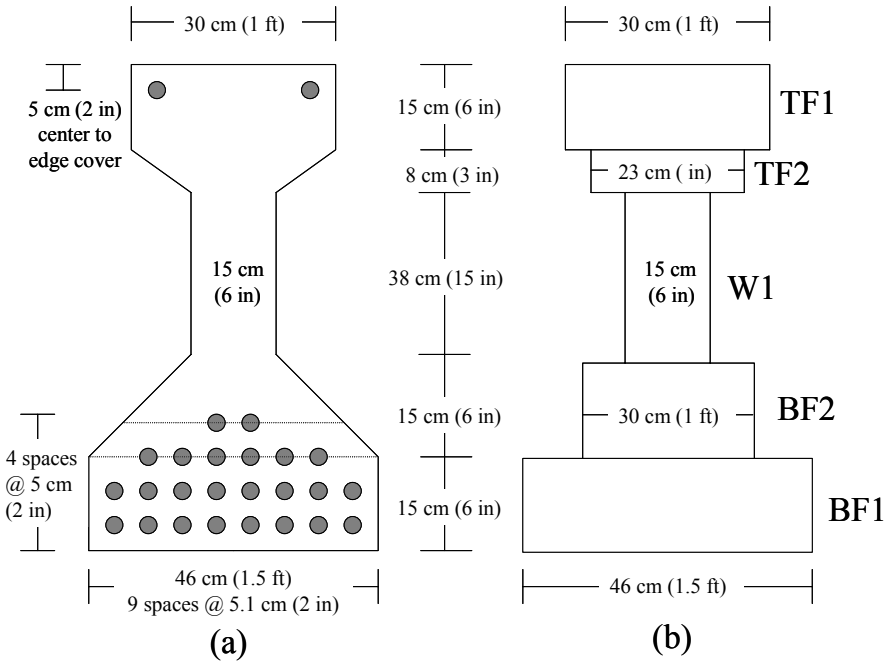

Fig. 4 Cross section of the AASHTO Type II Girder: (a) Actual Beam and (b) Idealized FE Simulation

A SIMPLIFIED MODEL OF PRESTRESSING

The AASHTO Type II girder is prestressed with 26 steel tendons, each 0.5 in (1.27 cm) in diameter, composed of low relaxation steel with σ_{Tu} = 270 ksi (1,860 MPa) strength and E_T = 29,000 ksi (200 GPa) stiffness[5]. Each prestressing tendon was initially loaded to 55% of its ultimate strength. Half of the tendons in the bottom flange were debonded for 3 ft (91 cm) from each end (FHWA, 2002). As depicted in Fig. 4, the prestressing tendons are not explicitly simulated in the finite element model. Instead, the equivalent effect of the tendons is modeled, that is (1) the prestressing forces and (2) the contribution of the tendons to the stiffness and strength.

To capture the effect of prestressing forces, an equivalent external pressure is applied at the ends of the girder, particularly on the bottom flange, BF1 and BF2, and the upper part of the top flange, TF1 (see Fig. 5(Top)). The prestressing pressure p is calculated according to:

$$p = 0.55(c_T \sigma_{Tu}) \quad (1)$$

where factor 0.55 refers to the level of prestressing in the tendons. Subscript "T" refers to the prestressing tendons; c_T is the volume fraction of the tendons in a particular cross sectional subdivision i (i.e. $c_T = A_T/A_i$ where A_T is the cross sectional area of the tendons in the subdivision and A_i is the total area of the subdivision) and σ_{Tu} = 270 ksi (1,860 MPa) is the strength of the tendons. In BF1, c_T = 3.0%, in BF2, c_T = 2.2%, and in TF1, c_T = 0.6%; c_T = 0% in the other cross sectional areas. Thus, the magnitude of p varies along the height of the girder according to the tendon concentration c_T.

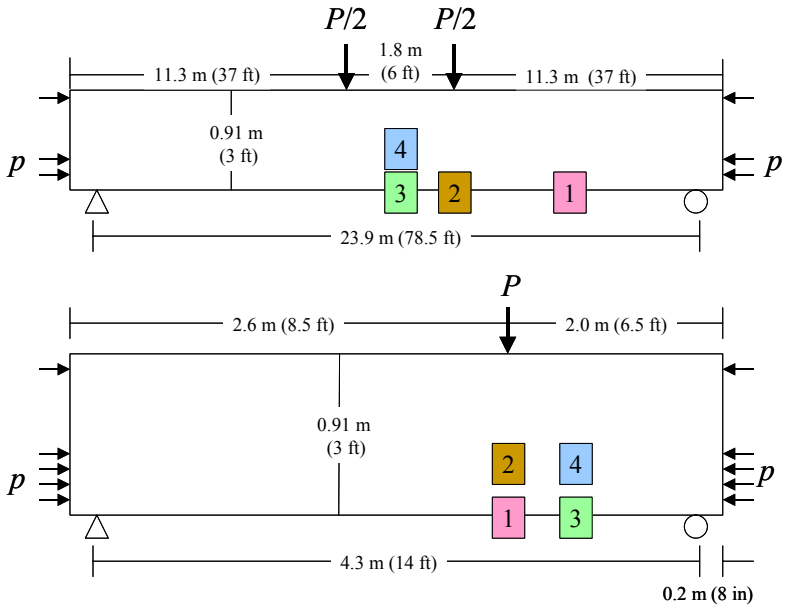

Fig. 5 Loading Configuration and Strain Gauge Locations for: (Top) The FHWA Flexure Test, (Bottom) The FHWA Shear Test

EFFECTIVE STIFFNESS AND STRENGTH OF THE BOTTOM FLANGE

At the structural level, the bottom flange is analogous to a composite material comprised of two homogeneous phases, the UHPC and the prestressing tendons. In this case, the stiffness of the bottom flange can be assigned an upper bound using the general rule of mixtures. In the simulations, the stiffness change due to the tendons is enforced through the stiffness of the composite fiber phase in the bottom flange C_F^B, while the composite matrix stiffness is kept constant:

$$C_F^B = C_F + c_T (E_T - C_F) \quad (2)$$

The presence of prestressing fibers also affects the composite yield strength of the bottom flange. Based on yield design theory, it can be shown that a lower strength bound of a uniaxially reinforced composite is simply the lower strength of the two composite components[6]. On the other hand, an upper strength bound as given by yield design theory is the weighted average of the composite components[6]. In the simulations, the upper strength

bound is applied to the yield strength of the composite fiber phase in the bottom flange f_y^B, while the composite matrix strength k_y is unchanged:

$$f_y^B \leq f_y + c_T(0.45\sigma_{Tu} - f_y) \quad (3)$$

where the factor 0.45 refers to the reserve strength in the prestressing tendons, i.e. 100%-55%.

For each case study, two different sets of material parameters were examined, a lower bound set and an upper bound set. Listed in Table 2 ("Base Case") is the lower bound model parameter set (which are equivalent to the DUCTAL^{TM} values in Table 1); Table 2 also highlights the modified upper bound values (in parentheses) in the "Base Case" row. As shown in Table 2, the values for σ_{Fc} are also increased to ensure $\sigma_{Fc} > f_y$, which is a requirement for stability of the 3-D strength domain (see [4] for details). The new values of σ_{Fc} were chosen to be arbitrarily larger than f_y, but since no compressive yielding occurred in the bottom flange of the FHWA tests, the exact value of this parameter is irrelevant.

	Modified UHPC Only Model Parameters (with Tendon Effect BF1/BF2)					
Ductility Parameter	M/M^0	C_F^B/M^0	f_t/k_y^0	k_y/k_y^0	f_y^B/k_y^0	σ_{Fc}/k_y^0
Base Case	1	0 (3.6/2.7)	0.1	1	0.67 (4.3/3.3)	1.4 (4.3/4.3)
R_K = .3%	0.1	0 (3.6/2.7)	0.1	1	0.67 (4.3/3.3)	1.4 (4.3/4.3)
R_K = 30%	14	0 (3.6/2.7)	0.14	0.96	0.71 (4.3/3.3)	1.4 (4.3/4.3)
R_D = 1	1	0 (3.6/2.7)	0.55	0.55	1.1 (4.7/3.8)	1.4 (4.8/4.3)
R_D = 10	1	0 (3.6/2.7)	0.01	1.1	0.58 (4.1/3.3)	1.4 (4.3/4.3)
R_S = 1.1	1	0 (3.6/2.7)	0.1	1	0.21 (3.8/2.9)	1.4 (4.3/4.3)
R_S = 3.5	1	0 (3.6/2.7)	0.1	1	2.9 (6.4/5.4)	3.6 (7.2/5.8)

Table 2 Normalized Values of UHPC Model Parameters Used in the FHWA Tests and Sensitivity Analyses. Changes from the Base Case Denoted in Bold. M^0 = 240 ksi (1.65 GPa); k_y^0 = 0.1 ksi (0.7 MPa)

RESULTS OF THE VALIDATION

The FHWA tests were numerically simulated to gauge the accuracy and reliability of the UHPC model. The finite element simulation was validated with the experimental data with respect to three different criteria:

- Load-deflection curves. The load-deflection curves of the FHWA specimen and the FE simulation demonstrated very good correlation (see Fig. 6). As shown in Fig. 6(a), the upper bound case accurately replicated the load-deflection behavior of the FHWA flexure test as the tendon stiffness and strength was activated. By contrast, Fig. 6(b) displays the aptness of the lower bound material parameters to model the FHWA shear test, as short tendon bonding lengths did not allow full activation of the stiffness and strength of the tendons. The simulated load-deflection curves and the experimental load-deflection curves for both FHWA case studies diverge when the

actual girders experienced structural failure. For the FHWA flexure test, this was due to tendon rupture; for the FHWA shear test, failure occurred as a result of tendon-UHPC interface failure.

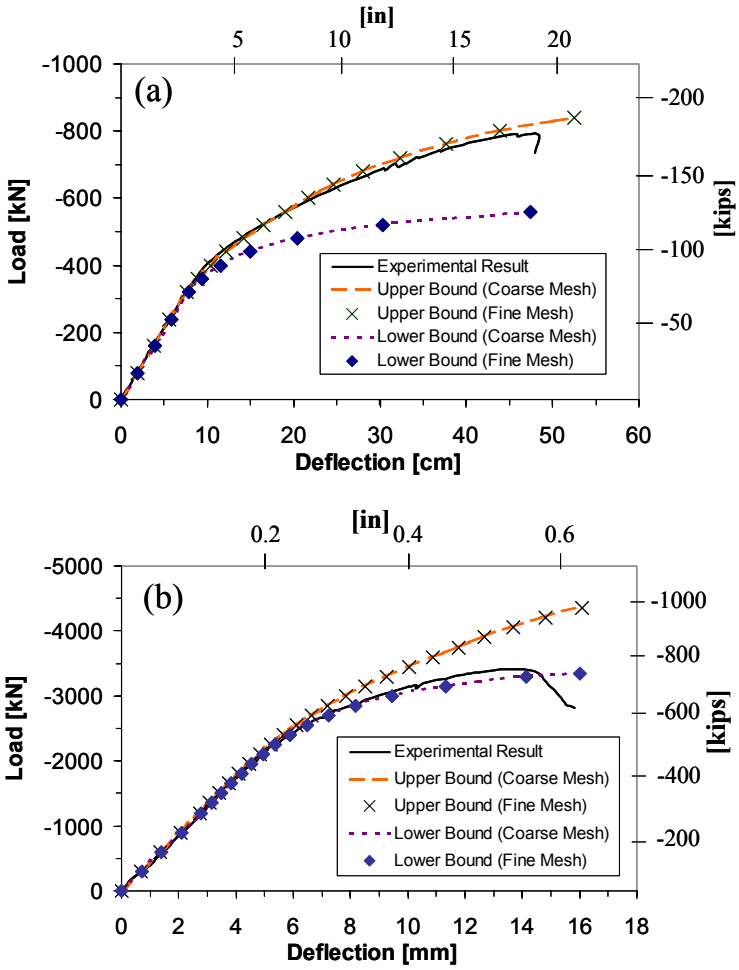

Fig. 6 Load-Deflection Results from the FHWA Simulations: (a) The FHWA Flexure Test (Deflection Measured at Midspan), (b) The FHWA Shear Test (Deflection Measured under Load Point).

- Strain gauge measurements. The FE program provides results for the deflection of the nodes in a given mesh during loading. Strain results are calculated as the change in distance between two nodes divided by the original distance between the nodes. Strain predictions obtained from the FE simulation exhibited excellent agreement with strain measurements from strain gauges placed at various locations (see Fig. 5) on the FHWA specimens.
- Cracking patterns. Plastic strains in the composite matrix ε_M^p can be related to cracking, which occurs in the cementititous matrix of UHPC. The composite matrix plastic strains as given by the FE simulation accurately modeled cracking observed in the FHWA specimens.

In this way, the UHPC model was shown to appropriately predict the behavior of UHPC structures not only at the global level, i.e. load-deflection behavior, but also the local level, i.e. strain and cracking results.

SENSITIVITY ANALYSIS OF DUCTILITY PARAMETERS

DETERMINING UHPC STRUCTURAL LIMITS

Two appropriate metrics for evaluating structural performance are the service limit and the ultimate limit. The service limit is the load P_s at which an acceptable service state is breached in the structure. For UHPC, this service state will be characterized by a maximum crack opening u. The ultimate limit is the highest load P_u which a structure can bear. This study is restricted to the evaluation of structural performance in terms of the service limit as the service limit lends itself to quantifying the structural performance of UHPC in terms of its model input parameters. As proven with the model validation, the FE implementation appropriately predicts the location and orientation of cracks in the structures. In addition, the FE program also provides an accurate numerical prediction of the total strain (plastic and elastic strain) for the case studies. Hence, the FE implementation offers a reliable prediction of principal composite matrix plastic strain $\varepsilon^{p}_{M,I}$ and, as a consequence, crack width[4].

Cracks can be categorized as unreinforced cracks or reinforced cracks. In the case of the FHWA tests, one may consider the shear cracks in the web to be unreinforced. The flexure cracks in the bottom of the flange, on the other hand, are reinforced with the prestressing tendons. Guidelines provided by the French Association of Civil Engineering (AFGC) suggest a limit for cracking in UHPC structures in the absence of reinforcement, provided here as a maximum composite matrix plastic strain $\varepsilon^{p,un}_{M,max}$: [7]

$$\varepsilon^{p}_{M,I} \leq \varepsilon^{p,un}_{M,max} = w_{max}/l_c \tag{4}$$

where l_c is a characteristic length, generally $l_c = (2/3)h$ where h is the height of the girder. w is the total cumulative crack opening measured over a length l_c; for common UHPC applications the maximum value of w for unreinforced cracks suggested by AFGC is w_{max} = 1/85 in (0.3 mm).

AFGC is less precise about guidelines for reinforced UHPC cracks. However, it is proposed that due to the supplemental safety supplied by the prestressing tendons, UHPC cracks may be allowed to grow to either a cumulative crack opening (measured over a distance l_c at which detrimental strain softening begins w_{soft}: [7]

$$w_{soft} = h/100 \tag{5}$$

or a cumulative crack opening (measured over a distance l_c) at which the reinforcing fibers (of length L_f) can no longer carry crack bridging stresses w_{lim}:

$$w_{lim} = L_f/4 \tag{6}$$

For the FHWA structures, where L_f = 0.5 in (13 mm) and h = 3 ft (910 mm), w_{lim} (< w_{soft}) provides a safer bound for cumulative crack widths for reinforced UHPC cracks. This

cumulative crack limit w_{lim} for reinforced UHPC cracks, rewritten in terms of composite matrix plastic strains $\varepsilon^{p,re}_{M,max}$, enforces the following condition:

$$\varepsilon^{p}_{M,I} \leq \varepsilon^{p,re}_{M,max} = L_f/4l_c \tag{7}$$

For the FHWA flexure and shear tests, $\varepsilon^{p,un}_{M,max} = 5\times10^{-4}$ and $\varepsilon^{p,re}_{M,max} = 5\times10^{-3}$.

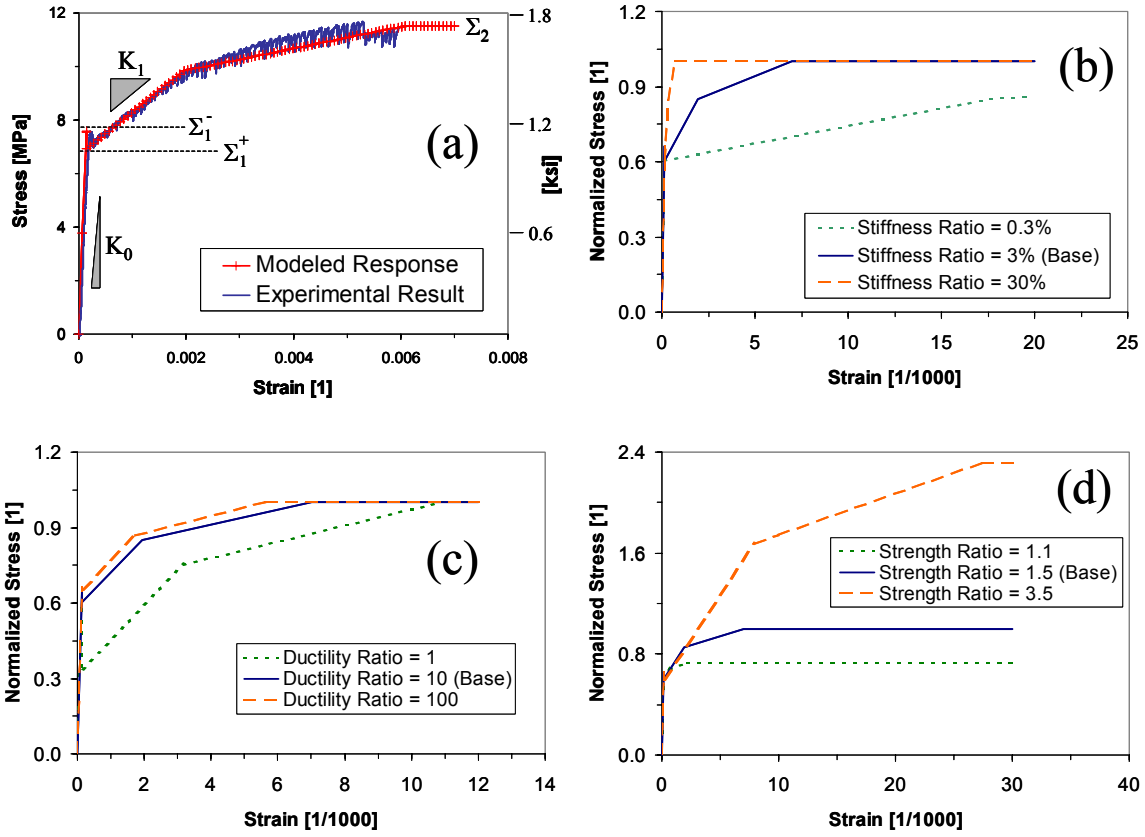

Fig. 7 Normalized UHPC Stress-Strain Behavior with Modified Ductility Parameters: (a) Tensile Stress-Strain Curve for "Base Case" UHPC (Data from Lafarge) Along with Modeled Response; (b) Modified Stiffness Ratios R_K; (b) Modified Ductility Ratios R_D; (b) Modified Strength Ratios R_S. Stresses in (b), (c), and (d) Normalized by Σ_2^0 =1.67 ksi (11.5 MPa).

For the ductility parameter sensitivity analysis which follows, the service load P_s is the applied load P on the FHWA structures at which either the maximum unreinforced composite matrix strain is first achieved $P_s = P(\varepsilon^{p}_{M,I} = \varepsilon^{p,un}_{M,max})$ in the web through shear cracking or the maximum reinforced composite matrix strain is first achieved $P_s = P(\varepsilon^{p}_{M,I} = \varepsilon^{p,re}_{M,max})$ in the bottom flange through flexural cracking.

DUCTILITY PARAMETERS

UHPC, as discussed, exhibits dramatic ductility improvements over normal fiber reinforced concretes when loaded in tension. The ductile stress-strain response for the UHPC "Base Case" is exhibited in Figure 7(a) along with the best-fit response given by the 3-D UHPC model. Here, the material behaves in a linear elastic manner (stiffness K_0) until first cracking occurs in the composite matrix at a macroscopic stress of Σ_1^-. Cracking is characterized by the post-cracking strength drop to a stress Σ_1^+. Upon further loading, the material strain-hardens quasi-bilinearly with an initial stiffness K_1. When a stress of Σ_2 is achieved in the material, the composite exhibits yielding behavior.

Ductility parameters are dimensionless combinations of the 3-D UHPC model parameters which characterize the post-cracking UHPC material behavior in relation to the initial (uncracked) UHPC material behavior as illustrated in Fig. 7(a). By altering the model parameters (see Table 2), the ductility parameters related to UHPC are modified to examine their effect on structural performance. Three ductility parameters are investigated in this chapter:

- Stiffness ratio, the ratio of post-cracking stiffness to initial stiffness (see Fig. 7(a)):

$$R_K \equiv K_1/K_0 \tag{8}$$

The stiffness ratio for the Base Case is $R_K = 3\%$. Two variations for the stiffness ratio are also studied in this chapter: $R_K = 0.3\%$ and $R_K = 30\%$. Since the effect of ductility is being evaluated, the virgin behavior of the material, i.e. the initial stiffness K_0, is kept constant. The material behavior for UHPC with the modified stiffness ratios is plotted in Figure 7(b).

- Ductility ratio, the ratio of residual strength to brittle strength during cracking in the composite matrix (see Fig. 2):

$$R_D \equiv k_y/f_t \tag{9}$$

For the Base Case, $R_D = 10$. Other ductility ratios investigated are $R_D = 1$ and $R_D = 100$. The first cracking strength Σ_1^- is kept constant, that is $k_y + f_t = \Sigma_1^-$. The UHPC stress-strain curves with modified ductility ratios are presented in Fig. 7(c).

- Strength ratio, the ratio of composite yield strength to the first cracking strength (see Fig. 7(a)):

$$R_S \equiv \Sigma_2/\Sigma_1^- \tag{10}$$

The strength ratio for the Base Case is $R_S = 1.5$. The two variations of the strength ratio studied in here are $R_S = 1.1$ and $R_S = 3.5$. The UHPC behavior with altered strength ratios is portrayed in Fig. 7(d).

The upper bound FHWA flexure test and the lower bound FHWA shear test were simulated with the altered ductility parameters. The assumptions and procedures for the new simulations are identical to those previously described except for changes to the material parameters (M, f_t, k_y, and f_y) to achieve desired ductility parameter values. The compressive strength of the composite fiber was also adjusted in some cases to maintain the stability of

the 3-D strength domain. The material parameters for these simulations are listed in Table 2 with the altered material parameters highlighted in bold font.

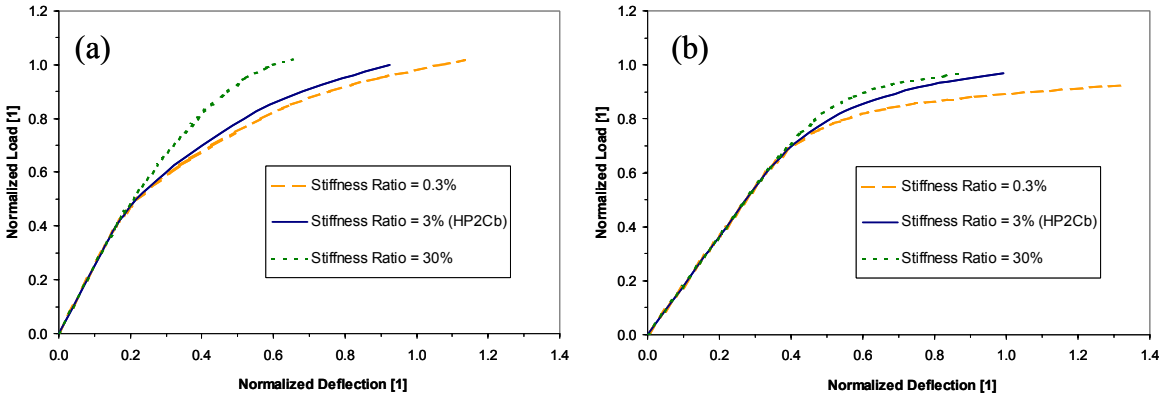

Fig. 8 Effect of Stiffness Ratio on Normalized Load-Deflection Behavior: (a) Upper Bound of the FHWA Flexure Beam. Deflection Measured at Beam Midpoint, Deflection Normalized by δ_u = 20 in (50 cm), Load Normalized by P_u = -180 kips (-800 kN). (b) Lower Bound of the FHWA Shear Beam. Deflection Measured at Load Point, Deflection Normalized by δ_u = 0.55 in (14 mm), Load Normalized by P_u = -765 kips (-3400 kN)

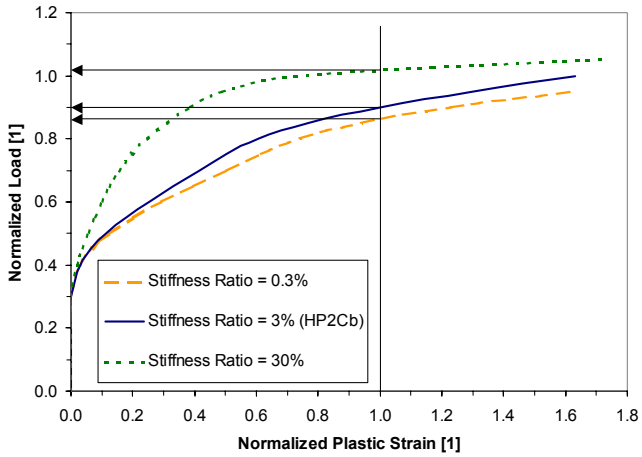

Fig. 9 Effect of Stiffness Ratio on Normalized Load-Maximum Crack Width Behavior of Upper Bound of the FHWA Flexure Beam. Cracking $\varepsilon^{p}_{M,I}$ measured in bottom flange, strain normalized by $\varepsilon^{p,re}_{M,max} = 5\times10^{-3}$, load normalized by P_u = -180 kips (-800 kN)

EFFECT OF STIFFNESS RATIO

The normalized load-deflection curves for the FHWA flexure and shear simulations with modified stiffness ratios are plotted in Fig. 8. The total loads P were normalized with the ultimate loads P_u as obtained in the FHWA experiments: for the flexure test P_u = -180 kips (-800 kN) when tendon failure occurred, for the shear test P_u = -765 kips (-3400 kN) when

tendon-UHPC bond failure evidently occurred. The deflections were normalized by the deflections at the ultimate loads $\delta_u = \delta(P = P_u)$: for the flexure test $\delta_u = 20$ in (50 cm), for the shear test $\delta_u = 0.55$ in (14 mm). As shown in Fig. 8, the stiffness ratios have some effect on the load-deflection behavior. In particular, an increase in stiffness ratio produces some improvement in the structural behavior of the FHWA flexure beam (Fig. 8(a)); a decrease in stiffness ratio has a softening effect on the structural behavior of the FHWA shear beam (Fig. 8(b)).

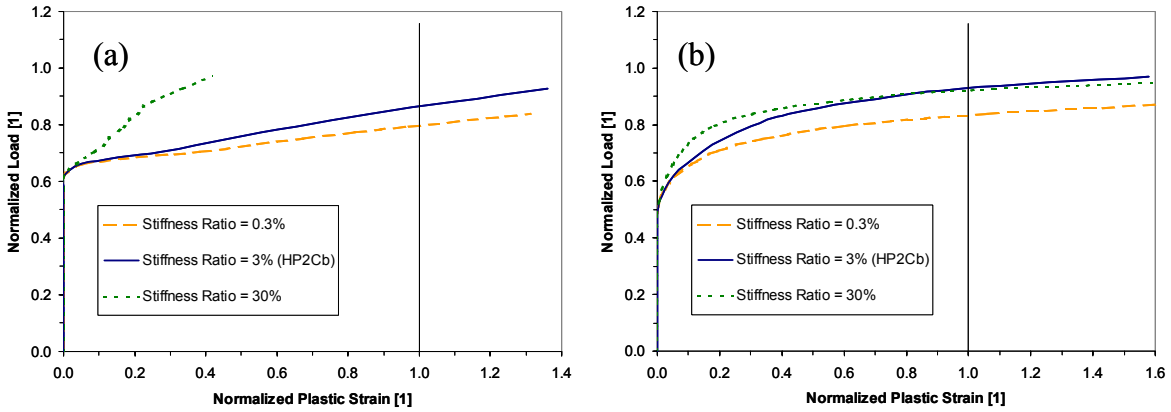

Fig. 10 Effect of Stiffness Ratio on Normalized Load-Maximum Crack Width Behavior of Lower Bound of the FHWA Shear Beam: (a) Flexure Cracking $\varepsilon^{p}_{M,I}$ Measured in Bottom Flange, Strain Normalized by $\varepsilon^{p,re}_{M,max} = 5\times10^{-3}$, Load Normalized by $P_u = -765$ kips (-3400 kN); (b) Shear Cracking $\varepsilon^{p}_{M,I}$ Measured in Web, Strain Normalized by $\varepsilon^{p,un}_{M,max} = 5\times10^{-4}$, Load Normalized by $P_u = -765$ kips (-3400 kN)

Altered Ductility Parameter	Normalized Load P_s/P_u FHWA Shear	FHWA Flexure
Base Case	0.87 (Web)	0.9
$R_K = 0.3\%$	0.8 (Web)	0.86
$R_K = 30\%$	1 (Flange)	1.02
$R_D = 1$	0.62 (Web)	0.86
$R_D = 100$	0.93 (Flange)	0.9
$R_S = 1.1$	0.85 (Flange)	0.87
$R_S = 3.5$	0.87 (Web)	1

Table 3 Normalized Loads at Service Limit for Ductility Parameters. Type of Failure for FHWA Shear Girder Listed in Parentheses.

By determining the load capacities of these structures at the service limit (maximum allowable crack width), these ductility parameter results become applicable on an engineering level. In Figs. 9 and 10 the normalized load is plotted against the normalized

maximum principal composite matrix plastic strain $\varepsilon^{p}_{M,I}$ for different stiffness ratios R_K. Flexural cracks in the flange are normalized with $\varepsilon^{p,re}_{M,max} = 5\times10^{-3}$, shear cracks in the web are normalized with $\varepsilon^{p,un}_{M,max} = 5\times10^{-4}$. In the case of the FHWA shear girder, significant cracking occurs in the reinforced bottom flange and unreinforced web[4]. Thus, Fig. 10(a) plots the load results in terms of flexural cracking in the (reinforced) bottom flange and Fig. 10(b) shows the load results in terms of shear cracking in the (unreinforced) web. Table 3 summarizes the normalized service loads P_s/P_u (as an example, highlighted with arrows in Fig. 9) which are achieved when the normalized composite matrix plastic strain $\varepsilon^{p}_{M,I}/\varepsilon^{p}_{M,max} = 1$ (demarcated with a vertical line in Figs. 9 and 10) for each structure. In the case of the shear girder, the lower service load limit as determined for bottom flange cracking and web cracking is listed in Table 3. Table 3 also clarifies the limiting crack type for the FHWA shear test in parentheses.

The service load limit P_s predicted for the Base Case (R_K = 3%, R_D = 10, R_S = 1.5) is lower than the ultimate load for both the FHWA flexure and shear girders, $P_s/P_u < 1$. In other words, although the FE simulations did not predict the ultimate loads, which were dictated by tendon or bond failure, the service limits suggested by AFGC are well below the ultimate load. Therefore, it appears that the FE simulations are able to provide safe service load limits despite neglecting complex tendon behavior.

These crack width limits may also propose safe structural service limits for any FRCC which is prestressed. In the case of the tendon rupture (as in the FHWA flexure test), crack width limits will also limit strains in the tendons. In the case of tendon slip, the crack width limits may prevent unsafe strain differentials between the tendon and the UHPC which induce tendon slip. In this way, it is inferred that the service limits ensure overall structural soundness, i.e. $P_s(R_K) < P_u(R_K)$. For example, in the case of the R_K = 30% for the flexure test, $P_s/P_u > 1$ as listed in Table 3. This, however, does signify that the ultimate load P_u for this stiffness ratio was achieved. Instead, since the service limit $\varepsilon^{p}_{M,I}/\varepsilon^{p}_{M,max} = 1$ also implies a safe limit on strains in the tendon, it is suggested that the ultimate load for this stiffness ratio is higher that the ultimate load of the actual FHWA flexure test $P_s(R_K = 30\%) > P_u(R_K = 3\%)$. Similarly, for the FHWA flexure girder with the lower stiffness ratio R_K = 0.3%, the normalized service load P_s/P_u = 0.86. This does not indicate that the structure has a reserve strength of (1-0.86)P_u. Instead, due to a faster development of flexure cracking $\varepsilon^{p}_{M,I}$ and, as a consequence, tendon strains, the tendons will most likely undergo rupture at a lower load, i.e. $P_s(R_K = 0.3\%) < P_u(R_K = 3\%)$. So P_s/P_u in Table 3 does not signify the reserve load capacity (or lack of load reserve capacity) in the FHWA tests with the varied ductility parameters. Instead P_s/P_u should merely be considered a measure with which to compare the service loads of the structures across variations in ductility parameters.

Table 3 reveals how changes in stiffness ratio affect the FHWA shear test more noticeably than the FHWA flexure test. This may be due to a "tendon effect", i.e. the effect of the prestressing tendon in the flexure test (the upper bound assumption) which masks flexural cracking effects in the flexure girder. Recall that this tendon effect is not as important in the shear test due to tendon slippage (hence the lower bound assumption). Also, the stiffness ratio seems to particularly affect the shear cracking as demonstrated in Fig. 10(b). This may be due to the more brittle cracking behavior in shear than in pure tension, as dictated by the larger stress drops in the composite matrix when the loading path is more compressive in

nature; a higher stiffness ratio may offset this brittleness. Accordingly, when the stiffness ratio is high, R_K= 30%, the governing mode of cracking changes from shear cracking in the web to flexure cracking in the bottom flange. One may conclude that this brittleness factor in shear may be mitigated by a favorable stiffness ratio more than the brittleness in tension.

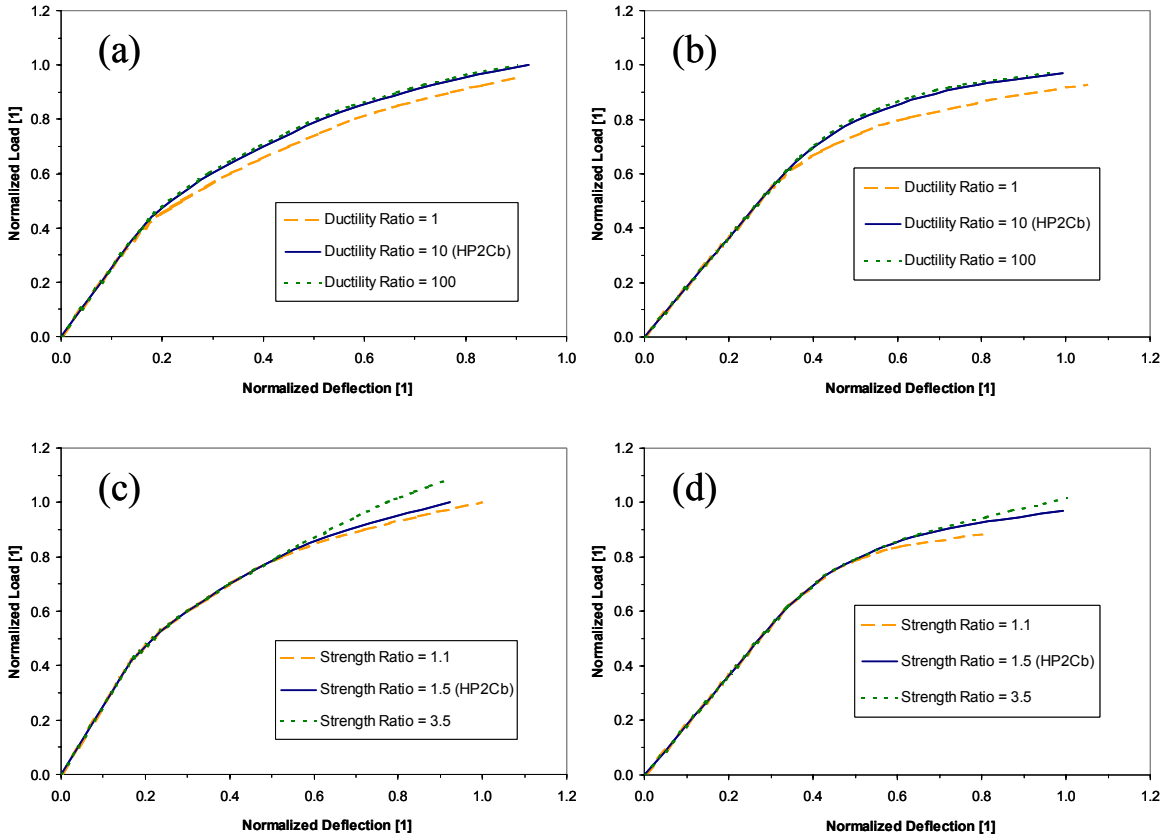

Fig. 11 Effect of Ductility Parameters on Normalized Load-Deflection Behavior: (a) Upper Bound of the FHWA Flexure Beam with Varying Ductility Ratios; (b) Lower Bound of the FHWA Shear Beam with Varying Ductility Ratios. (c) Upper Bound of the FHWA Flexure Beam with Varying Strength Ratios; (d) Lower Bound of the FHWA Shear Beam with Varying Strength Ratios. For FHWA Flexure Beam: Deflection Measured at Beam Midpoint, Deflection Normalized by δ_u = 20 in (50 cm), Load Normalized by P_u = -180 kips (-800 kN). For FHWA Shear Beam: Deflection Measured at Load Point, Deflection Normalized by δ_u = 0.55 in (14 mm), Load Normalized by P_u = -785 kips (-3400 kN)

EFFECT OF DUCTILITY RATIO

Figures 11(a) and (b) display the effect of ductility ratio on the load-deflection behavior of the FHWA tests. From these load-deflection curves, it appears that increasing the ductility ratio has a negligible effect on the load carrying capacity while decreasing the ductility ratio has a significant effect on the load carrying performance of these structures. This may be due to the insignificant effects that large enhancements in ductility ratio actually have on the stress-strain behavior of UHPC. As shown in Fig. 7(c), an improvement in ductility ratio

from R_D = 10 to R_D = 100 has a small effect on the stress-strain behavior (compare to the decrease of ductility ratio from R_D = 10 to R_D = 1).

The effect of changes in ductility ratio R_D on the service load limit P_s is summarized in Table 3. As implied by the results in Table 3, changes in ductility ratio have little effect on the FHWA flexure test. As in the case of changes in stiffness ratio, this may be due to the overwhelming tendon effect which diminishes flexural cracking in the bottom flange. The ductility ratio, on the other hand, has a considerable influence on the service load of the FHWA shear girder, particularly with regard to shear cracking (see Fig. 12). As in the case of stiffness ratios, it appears that increases in ductility ratio have a substantial mitigating effect on the brittleness of UHPC cracking in shear. For this reason, a larger ductility ratio R_D =100, despite having a small effect on stress-strain behavior, causes a shift in governing cracking behavior from shear cracking in the web to flexure cracking in the bottom flange for the FHWA shear test.

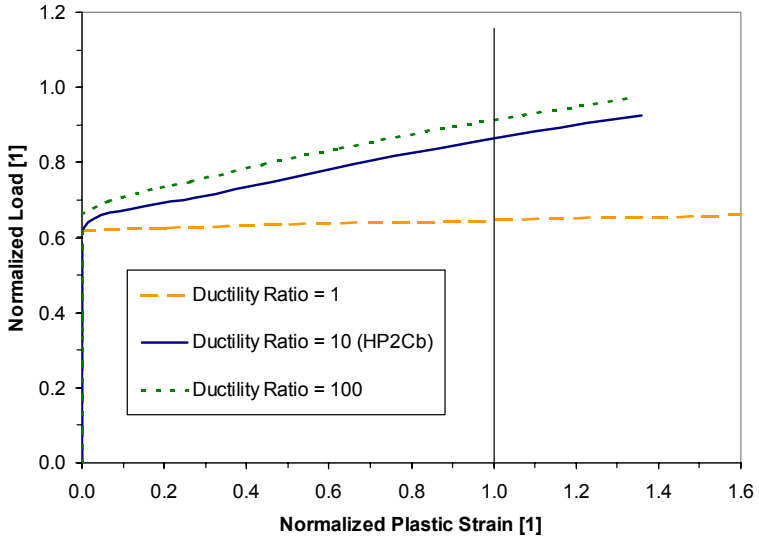

Fig. 12 Effect of Ductility Ratio on Normalized Load-Maximum Crack Width Behavior of Lower Bound of the FHWA Shear Beam for Shear Cracking. $\varepsilon^{p}_{M,I}$ Measured in Web, Strain Normalized by $\varepsilon^{p,un}_{M,max} = 5\times10^{-4}$, Load Normalized by P_u = -785 kips (-3400 kN)

It is interesting to note how a poor ductility ratio induces unstable shear cracking in the FHWA shear beam. Fig. 12 shows how at lower ductility ratios R_D = 1, the shear cracks propagate in an unstable manner upon achieving a normalized load of P_s/P_u = 0.62. The low ductility ratio is characteristic of a strain-softening FRCC. Therefore, while UHPC (Base Case) induces post-cracking hardening at a structural level, a shear beam composed of poor FRCC would undergo unsafe shear cracking without shear reinforcement. Conversely, in general, UHPC girders do not require shear reinforcement due to the high ductility ratio inherent in UHPC.

EFFECT OF STRENGTH RATIO

The effect of the strength ratio R_S on the load-deflection behavior of the FHWA tests is exhibited in Figs. 11(c) and (d). For both FHWA tests, the effect of the strength ratio manifests itself at higher loads and deflections than the other ductility parameters as the maximum material strength of UHPC is untapped at lower post-cracking loads. From the load-deflection curves, it appears that the structural behavior of the flexure test is noticeably improved with an increase in strength ratio, but is unaffected by a strength ratio reduction. Conversely, the shear girder shows insignificant structural improvement with an augmentation of the strength ratio, while exhibiting poorer load carrying capacity when the strength ratio is decreased.

The service load limits for both tests are listed in Table 3. As shown for the FHWA flexure test, a drop in strength ratio induces, as expected, minor changes to the service load limit P_s for the FHWA flexure test. This is most likely due to the tendon effect which makes the drop in strength ratio imperceptible at a structural level. Conversely, an increase in the strength ratio has a structural strengthening effect on the FHWA flexure girder. Disregarding the probability of tendon failure for the moment, Fig. 11(c) implies that an increase in strength ratio can significantly enhance the ultimate capacity of the flexure girder. However, for a very large increase in the strength ratio (R_S = 1.5 to R_S = 3.5), there is not a commensurate increase in the service load limit (P_s/P_u = 0.9 to P_s/P_u = 1). Moreover, it is the service limit, not the ultimate limit, which should govern the design of real world UHPC applications. Thus, it appears that the economic cost of achieving higher strength ratios for UHPC may be wasted in prestressing applications with large tendon effects.

For the FHWA shear test, changes in strength ratio have no effect on shear cracking. That is, even a sizeable increase in tensile strength will have a small effect on the shear strength. Accordingly, in the case of the FHWA shear beam, the large change in strength ratio does not have any bearing on structural shear cracking. On the other hand, when the strength ratio is reduced, the flexure capacity of the shear girder is diminished to such a degree that flexural cracks govern the service load limit.

CONCLUSIONS

Using a previously developed UHPC model and finite element implementation, which were shown to give accurate prediction of the behavior of UHPC structure, a sensitivity analysis of UHPC ductility was presented. The ductility parameter sensitivity analysis outlined in this paper provides insight into how UHPC ductility manifests itself at the structural level:

- Changes in stiffness ratio appear to have modest effects on the structural performance of UHPC flexure and shear girders. However, a large increase in the stiffness ratio may change the mode of cracking failure in shear girders from shear cracking in the web to flexural cracking in the bottom flange as shear cracking appears to be especially sensitive to changes in the stiffness ratio.
- Increases in ductility ratio of UHPC will have negligible effects on flexure girders due to the tendon effect. However, since shear cracking is highly sensitive to changes

in the ductility ratio, the ductility ratio is an important factor in shear girder applications.

- It is the high ductility ratio of UHPC which makes the elimination of the shear stirrups in UHPC structural applications possible. As shown, a drop in ductility ratio will lead to unstable shear cracking in the shear girder.
- Increases in strength ratio have positive effects on the performance of the prestressed girders, but perhaps not in proportion to the cost of attaining these strength gains. In other words, it appears that in the case of prestressed flexure girders, the prestressing already masks some of these strength gains. Therefore, possible future improvements in tensile strength should also be combined with structural designs which exploit these material advantages.
- In the case of the shear girder, improvements in the strength ratio have little structural effect as increases in the strength ratio have muted effects on the shear strength. Again, any improvements to the strength ratio may be squandered for certain structural applications.

More generally, this sensitivity analysis also suggests ways that UHPC can be used more efficiently. For example, in some cases, the service load limit governed by shear cracking is much lower than the service load limit governed by flexure cracking. For this case, the prestressing tendons are wasted, as their presence does not improve structural performance. The most efficient structural design for exploiting UHPC capacity would be for instances where the service load limit governed by shear cracking was equivalent to that governed by flexure cracking. However, this is only one criterion for efficient use of UHPC material advantages, not economic efficiency of the construction of an UHPC structure.

ACKNOWLEDGEMENTS

This research was performed as a part of a research collaboration with Lafarge-Bouygues-Rhodia Industry with Dr. Paul Acker as Program Director. The authors also gratefully acknowledge the assistance and experimental data provided by the FHWA through Joey Hartmann.

REFERENCES

1. ductal.com web site, 2001.
2. imagineductal.com web site, (2001).
3. Chuang, E., and Ulm, F.-J., "A Two-Phase Composite Model for High Performance Cementitious Composites and Structures," *ASCE Journal of Engineering Mechanics*, V. 128, No. 12, 2002, pp. 1314-1323.
4. Chuang, E., and Ulm, F.-J., "Ductility Enhancement of High Performance Cementitious Composites and Structures," *MIT-CEE Report R02-02 to the Lafarge Corporation*, 2002.
5. American Association of State Highway and Transportation Officials (AASHTO), *Interim Standard Specifications for Highway Bridges*, 2000, American Association of State Highway and Transportation Officials, Washington, D.C.

6. Ulm, F.-J., and Coussy, O, *Mechanics and Durability of Solids, Volume I: Solid Mechanics*, 2002, Prentice-Hall, Upper Saddle River, New Jersey.
7. Association Française de Génie Civil (AFGC), *Ultra High Performance Fibre-Reinforced Concretes*, 2002, AFCG.